The University of Queensland

Bachelor of Engineering Thesis

Preliminary Investigation of Remote Sensing
for Concentrating Solar Thermal Plants

Student Name: Byron BURGESS–GALLOP
Course Code: MECH4500
Supervisor: Dr Andras Nagy
Submission Date: 28 October, 2016

A thesis submitted in partial fulfilment of the requirements of the
Bachelor of Engineering Degree in Mechanical Engineering

UQ Engineering

Faculty of Engineering, Architecture and Information Technology

ABSTRACT

This investigation considers the technical feasibility of applying and automating remote sensing techniques to estimate the solar-weighted specular-reflectance of heliostats within Concentrating Solar Thermal (CST) plants. The primary remote sensing technique investigated uses a visible-range imaging sensor to estimate the reduction in specular reflectance of a soiled heliostat, assuming that this is approximately proportional to the increase in diffuse reflectance measured. Experiments were performed with a digital single-lens reflex (DSLR) camera with a flash and 12-bit charge coupled device (CCD) sensor. The experiments were set up to simulate different relative positions between a heliostat and the sensor lens. The captured images were then processed to estimate the mean diffuse reflectance. The results clearly distinguish a clean heliostat from a soiled heliostat (> 5% reduction in specular reflectance) by the relative difference in the mean diffuse reflectance. This result can also be obtained by processing the change in the standard deviation of the diffusive reflectance distribution. Additional processing methods are suggested that may provide quantitative absolute measurements capable of being integrated into an automated unmanned aerial vehicle (UAV).

A solar reflectometer was also used to determine the optical characteristics of different dust compositions with respect to different wavelength bands and heliostat reflector surfaces. The results were able to characterise the behaviour of different wavelengths with respect to a solar-weighting. The results also confirmed the initial assumption that the reduction in specular reflectance is approximately proportional to the increase in diffuse reflectance measured. Empirical linear relationships were derived for the change in specular reflectance as a function of change in diffuse reflectance. These relationships were found to hold between different reflector surfaces and vary between different dust compositions. The technique investigated is capable of being applied to areas of different dust compositions, assuming the dust can be optically characterised and does not change significantly over time. The accuracy of this method is dependent on the instrumentation and the optical characteristics of the representative soiling dust. Uncertainties may arise any due to spacial and temporal variations of dust composition at a particular CST plant. In summary, the development of this remote sensing technique has the potential to increase the current coverage and time resolution of reflectance measurements required to better optimise the cleaning of CST plants for cost effectiveness.

ACKNOWLEDGEMENTS

To Dr Andras Nagy, many thanks for offering an interesting topic of research. Your guidance throughout the year has proved valuable and is greatly appreciated.

To Dr Yuanshen Lu, thank you for your assistance with collecting and interpreting the reflectometer data, even at short notice.

To Edward Greenaway, thank you for your support and always taking a keen interest in each challenge that arose.

To my family and friends, thank you for the encouragement and being the motivation to submit this thesis.

CONTENTS

LIST OF FIGURES

LIST OF TABLES

1 INTRODUCTION

1.1 BACKGROUND

The manual measurement of heliostat specular-reflectance is often a routine procedure at concentrating solar thermal (CST) plants. In some environments the dust that accumulates on heliostats can lower the specular reflectance exponentially over time (Fernández-Reche 2006). This reduces the amount of solar energy reaching the receiver and therefore reduces power production. Knowledge of the individual heliostat reflectance at different moments in time can therefore be used to optimise the cleaning procedure for cost effectiveness (ASTRI 2015). Manual measurements, however, are labour intensive and time consuming, given the scale of CST plants. They are also highly localised, meaning that one measurement alone is not necessarily representative of the heliostat area. The existing measurement method therefore limits the spacial extent and temporal resolution of reflectance measurements, and therefore the effect to which the cleaning procedure is optimised. This investigation considers the technical feasibility of applying and automating remote sensing techniques to estimate the specular reflectance of heliostats within CST plants.

1.2 AIMS

This investigation aims to assist in improving the operational efficiency of CST plants by increasing the spacial extent and temporal resolution of specular reflectance data for heliostats.

1.3 OBJECTIVES

The primary objective of this investigation is to propose and validate a remote sensing method capable of increasing the spacial extent and temporal resolution of specular reflectance data for heliostats. The secondary objective of this investigation is to demonstrate the processing of remotely sensed data that is simulated to have been captured by a UAV.

1.4 SCOPE

This investigation considers the requirements of existing analogue and digital sensors for future integration into an automated UAV system. The use of existing remote sensing software, such as ENVI, is considered for the data processing tasks. High-level programming languages with open source image processing libraries, such as Python, are also considered for the data processing tasks. Heliostat soiling, due to dust particles, is the primary process of interest. Degradation of the reflecting surface itself is out of scope due to the longer time periods required to equal the negative effect of soiling. An investigation relating to the design of a suitable UAV is being researched simultaneously by Edward Greeanaway, and is out of scope in this investigation. The design of new electrical input circuits and optics is also out of scope due to time constraints.

2 LITERATURE REVIEW

2.1 CST ENERGY PRODUCTION

CST energy is produced using solar collectors to focus the Sun's energy onto one or more solar receivers. A study by Kalogirou (2004) has categorised the different types of solar collector designs and described each type. Collector designs can broadly be categorised as stationary or sun tracking. Stationary collectors are subcategorised as either flat-plate, compound parabolic or evacuated tube collectors. Sun tracking collectors are subcategorised as either parabolic trough, linear Fresnel, parabolic dish or heliostat field collectors. Heliostat field collectors were selected as the primary solar collector of interest in this preliminary investigation, due to the known problem of soiling associated with these collectors (ASTRI 2015) and their simple design.

Heliostat field collector designs have also been described by Kalogirou (2004). A single heliostat is made up of one or more mirror segments, known as facets, that are mounted upon a sun-tracking, dual-axis mount. The mount is designed such that incident sun rays are reflected onto a central radiative-convective heat exchanger, known as the central receiver. This general layout, shown in Figure 1, is referred to as a Central Receiver System (CRS). In practice, heliostats are distributed in one of two ways (Kalogirou 2004). In one such configuration, the heliostats surround a cylindrical central receiver in all directions, which is the configuration shown in Figure 1. Another configuration exists where heliostats are positioned only on the polar side of a cavity type central receiver (e.g. south of the receiver in the southern hemisphere). In this configuration the lower angles of incidence collect a higher proportion of the Sun's Direct Normal Irradiance (DNI). The type of CRS configuration and the height of the central receiver will influence the design of the heliostat field.

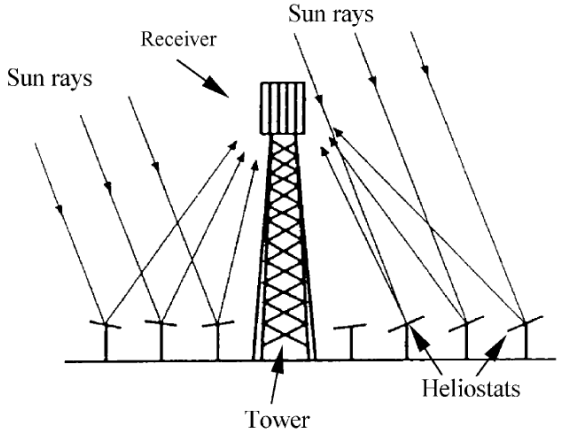

Figure 1 – Layout of a CST central receiver system (Kalogirou 2004)

Kalogirou (2004) has also listed typical CRS operating parameters. In a CRS the concentration ratio is proportional to the number of heliostat collectors, and typically in the range of 300 – 1500. Typical heliostat surface areas range between 50 to 150 m^2. Reflectance has been identified as a critical parameter affecting operational efficiency. The concentration ratio and reflectance together determine the solar flux at the central receiver, which is typically in the range of 200 to 1000 kW/m^2. These parameters presented by Kalogirou (2014) are useful as initial values to estimate the effect of soiling, however, little context is given. In order to achieve a best estimate of soiling effects in Australia, operating parameters are required with context such as location, latitude, Direct Normal Irradiance (DNI), thermal energy production and net electrical energy production.

In Australia there is currently only one CSP plant supplying electricity to the grid. Vast Solar's $25 million Jemalong pilot plant (Vast Solar 2015) has a peak thermal energy production of 6 MW_{th} and a peak electrical energy production of 1.1 MW_e. Unlike traditional CRS plants it uses a modular design consisting of 5 heliostat-receiver modules, as shown in Figure 2. Each module contains 700 heliostats to the south of a billboard-style receiver. Each receiver has a surface area of 2 m^2 mounted at a height of 25 m (Coventry et al. 2014). The receivers use sodium as a heat transfer fluid with an inlet temperature of 270 $°C$, outlet temperature of 560 $°C$ and a peak flux of 1.5 MW/m^2. The sodium at the receiver output is used to heat molten salt for storage in insulated tanks. The molten salt from the storage tanks is then used to heat water into steam, for use in a conventional steam turbine power cycle. This method of supplying thermal energy to the steam turbine can continue to generate electricity for up to 3 hours without heating at the central receivers. The aim of the Jemalong pilot plant is to demonstrate the concept of modular CSP over a 30-year project life (Vast Solar 2015). Although this plant is not at a commercial scale, plans are underway to commission a $90 million, 30 MW_{th} commercial plant using 90 modules. These operating parameters are therefore useful as a standard case for estimating the effect of soiling on a commercial scale CSP plant.

Figure 2 – Vast Solar's modular central receiver pilot plant (Sparks 2016)

2.2 HELIOSTAT CLEANING

The most recent report published by the Australian Solar Thermal Research Initiative (ASTRI 2015) again highlights the potential to reduce costs by optimisation of the cleaning procedure. The approach taken by ASTRI to reduce cleaning costs involves both monitoring and characterising the soiling of heliostats. This investigation will adopt a similar approach. However, rather than monitoring the rates of soiling in a natural environment, soiling will be simulated by manually applying dust to the surface (discussed in Section 3) due to time constraints.

ASTRI (2015) also mentions that the soiling data will be used to generate soiling models that will help optimise the cleaning schedule. It was noted that the monitoring is performed on a small sample size of test heliostats, smaller in scale than a commercial CST plant. Although the results are not yet known, it is possible that the data and subsequent models generated will be specific to the environmental conditions from where the data was collected. In this case the importance of developing a remote sensing method would be highlighted. Being able to accurately capture the complete field of heliostats at regular intervals in times would allow for the quick collection of environment specific data to build more accurate models.

2.3 REFLECTANCE MEASUREMENTS

Unfortunately, due to the weight and requirement for optical precision, using an integrating sphere type reflectometer is not viable for UAV remote sensing. Optical imaging sensors are therefore a better starting point for investigation, assuming they can be dampened. A significant challenge with this method, however, is the processing of the images. It is still useful to understand the operating principles of an integrating sphere, as this type of instrumentation can be used to calibrate imaging methods.

Modern reflectometers, such as those based on an integrating sphere, are generally compliant to standards such as ASTM E903 (2012) and G173 (2012). ASTM E903 specifies the geometry and instrumentation of the integrating sphere. An integrating sphere refers to a sphere with a highly diffuse inside surface. Any light that enters the sphere bounces in many different directions. Some fraction of the light energy will be absorbed at a baffled sensor, and some will be absorbed by the specimen being measured. The input light energy is usually that of a specular laser, such as is the case with the 410-Solar Reflectometer (Surface Optics Corporation 2016). At the known location of the specular beam reflected by the specimen, a port can either be opened (to let specular reflection escape) or closed (to trap both diffuse and specular reflections within the sphere). When the port is opened, diffuse reflectance is therefore measured. When the port is closed, the total reflectance is measured (diffuse and specular). The specular reflection of the specimen is therefore calculated as the difference between the total reflection and the diffuse reflection.

In a multispectral reflectometer, such as the 410-Solar, these reflectance values are calculated for each bandwidth. The ASTM G173 specifies the weightings that must be applied to each bandwidth to represent the reflectance of solar energy under standardised atmospheric conditions. The solar weighted reflectance is therefore the reflectance value of interest when considering the efficiency of CST power generation. The following section considers the feasibility of estimating the solar weighted reflectance using optical bandwidth (red, green and blue) sensors.

3 REFLECTOMETER DATA

3.1 METHODS

Multispectral reflectance data was collected in order to identify and characterise effects that are expected to vary between CST plants. The effects tested for were those relating to differences in reflector surface types (back surface vs front surface) and dust compositions (light shades vs shades). Four different types of reflector surfaces were tested. These included three back surface mirrors of varied coating thicknesses (6mm glass, 3mm glass and 1mm acrylic). An aluminium alloy front surface mirror was also tested. Figure 3 shows the different characteristic of each surface type. The main point of interest is whether refractive effects will make it difficult to characterise the reflections, particularly on the standard back surface mirrors. Two dust compositions of qualitative difference were also tested. One was a light-shade lime-soil (carbonate rich) fertiliser. It can also be described as well sorted and fine grained. The other dust was dark-shade garden soil (organic rich). It can be further described as poorly sorted and fine to medium grained.

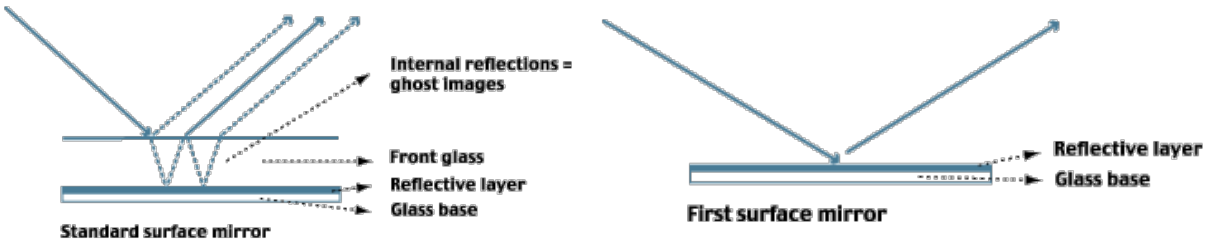

Figure 3 – Different reflector surfaces types showing refractive effects (DNP Denmark 2016)

The instrument used to collect the data was a 410-Solar Reflectometer (Surface Optics Corporation). The spectral resolution of this sensor is shown in Table 1.

Band #	Name	Range [nm]		Mean Wavelength [nm]	Mean Colour Description
1	UV	335	380	358	Near Ultraviolet
2	VIS 1	400	540	470	Blue
3	VIS 2	480	600	540	Green
4	VIS 3	590	720	655	Red
5	NIR	700	1100	900	Near Infrared
6	SWIR 1	1000	1700	1350	Shortwave Infrared 1
7	SWIR 2	1700	2500	2100	Shortwave Infrared 2
8	Solar	335	2500	N/A	N/A

Table 1 – Spectral resolution of 410-Solar reflectometer (Surface Optics Corporation)

The collection of reflectance data was performed using a 410-Solar Reflectometer (Surface Optics Corporation 2016). Each of the mirror types were tested in at least one clean state in two soiled states (see Appendix A for tabulated data). Each state was also characterised by a mean of at least three reflectometer measurements across different locations on the surface. The cleaning was kept consistent by gently dusting the surface with a soft cloth, followed by applying methylated spirits and wiping clean with a microfiber cloth. The mirrors were cleaned this way before each clean test, and before applying dust to the surface. The dust was applied by placing a spoonful directly on the surface and then tilting and tapping the mirror until an even layer had adhered. The mirror was then tipped upside down to removes excess dust, leaving a fine static coating of dust. The experiments were performed over different days to recognised if there were any lab related biases. The humidity is believed to influence the amount of dust that sticks statically to the surfaces.

3.2 RESULTS

3.2.1 Spectral Signatures of Second Surface Reflectors

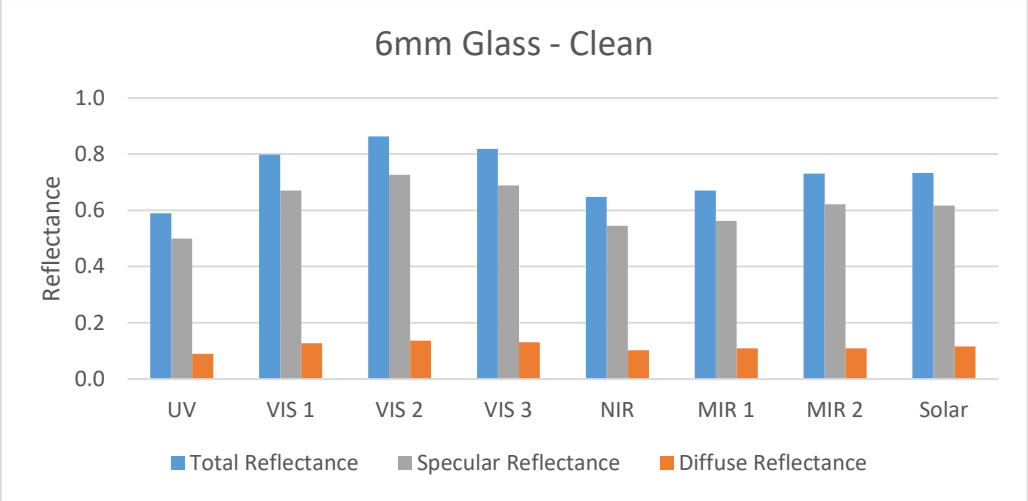

Figure 4 – Mean reflectance values of a clean 6mm glass mirror

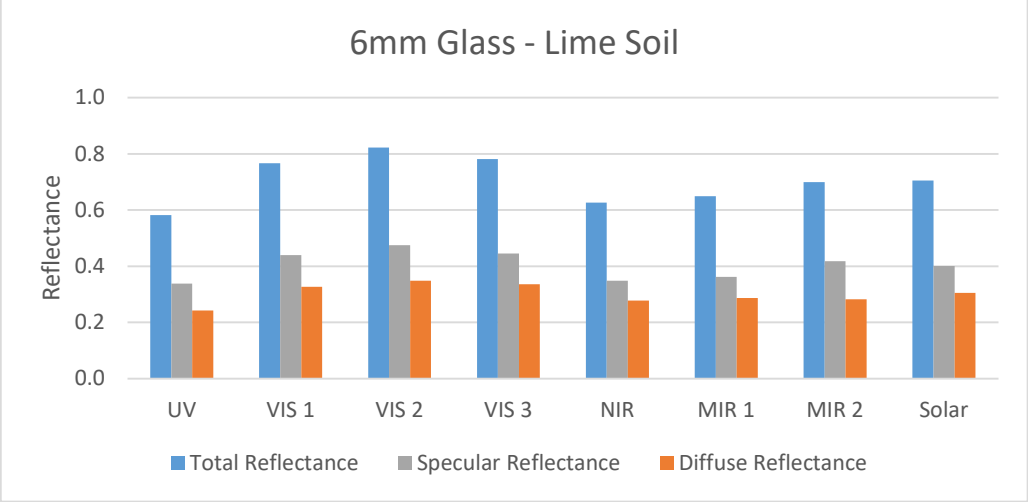

Figure 5 – Mean reflectance values of a 6mm glass mirror soiled using lime soil

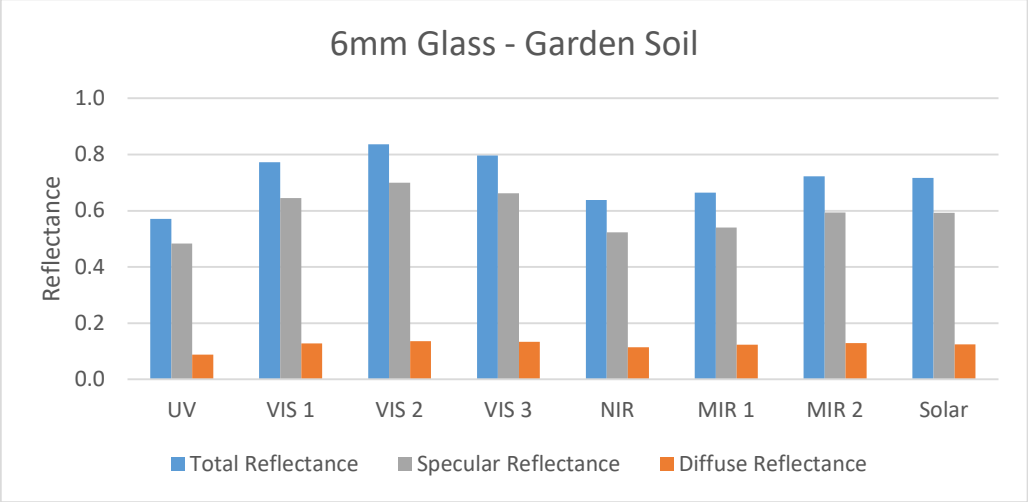

Figure 6 – Mean reflectance values of a 6mm glass mirror soiled using garden soil

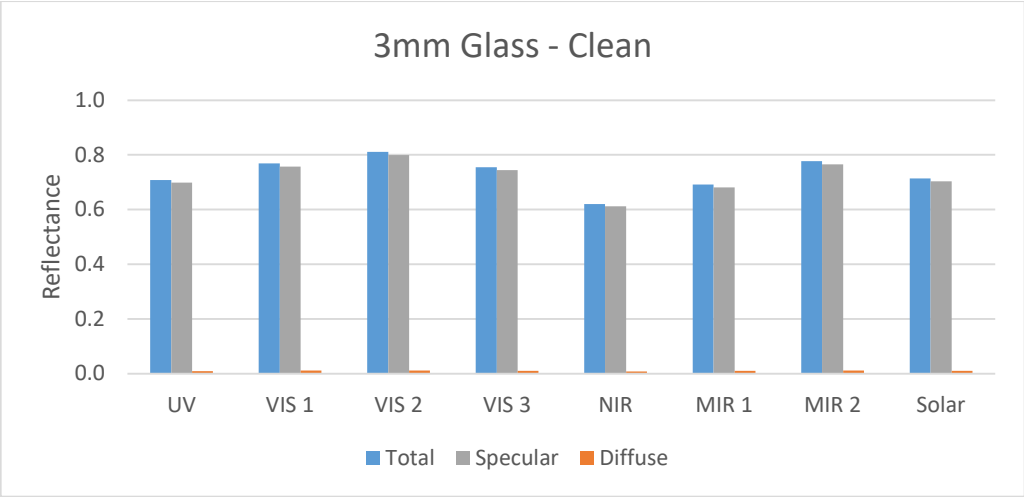

Figure 7 – Mean reflectance values of a clean 3mm glass mirror

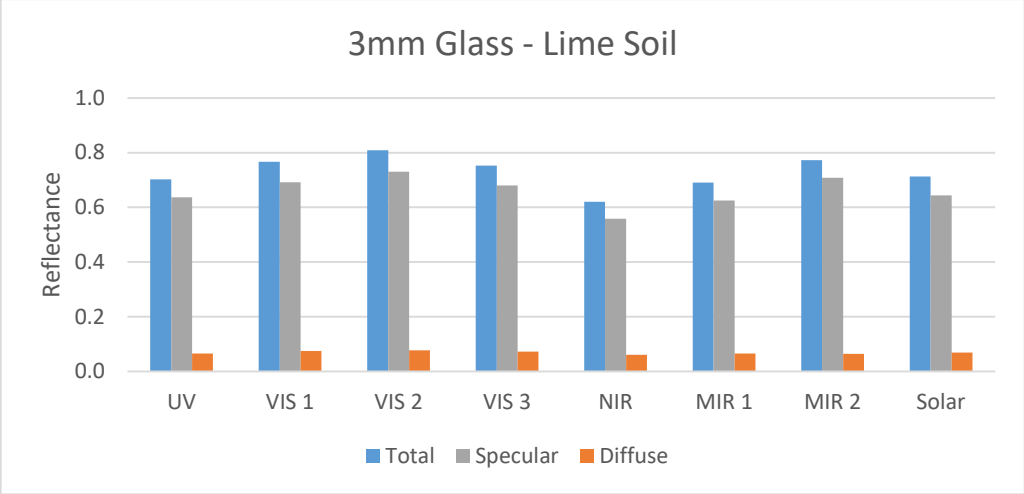

Figure 8 – Mean reflectance values of a 3mm glass mirror soiled using lime soil

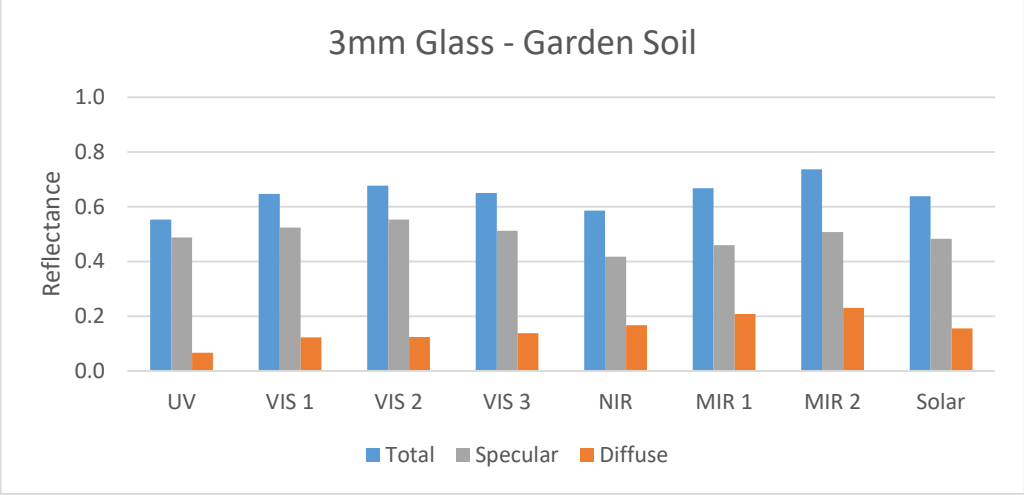

Figure 9 – Mean reflectance values of a 3mm glass mirror soiled using garden soil

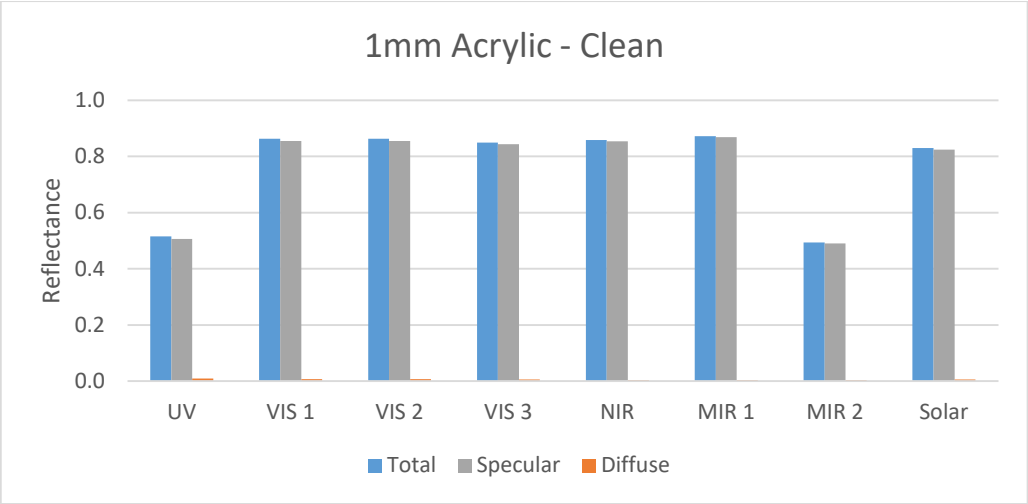

Figure 10 – Mean reflectance values of a clean 1mm acrylic mirror

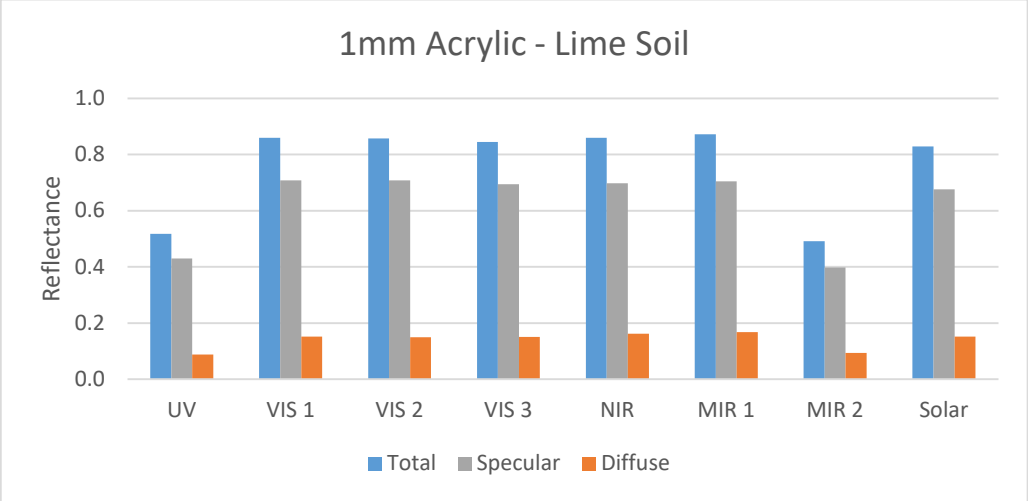

Figure 11 – Mean reflectance values of a 1mm acrylic mirror soiled using lime soil

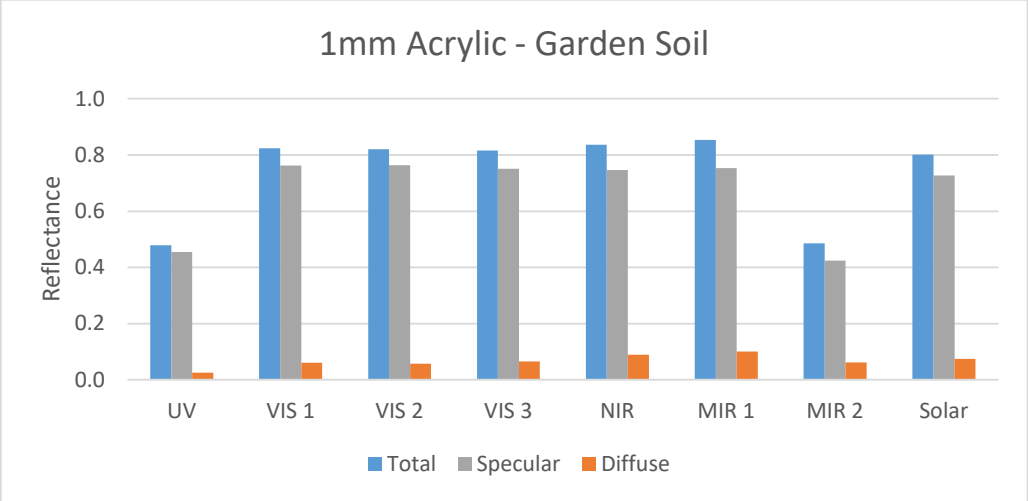

Figure 12 – Mean reflectance values of a 1mm acrylic mirror soiled using garden soil

3.2.2 Spectral Signatures of First Surface Reflector

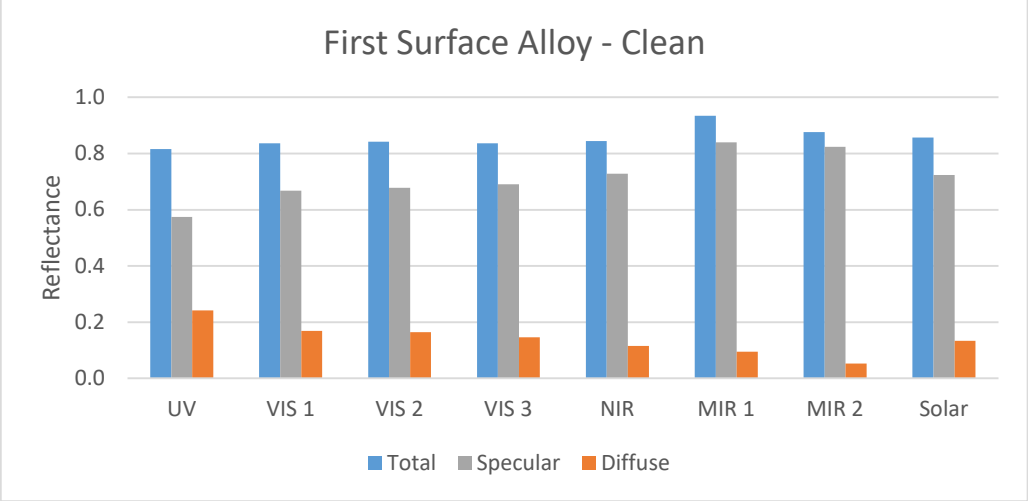

Figure 13 – Mean reflectance values of a clean first surface alloy mirror

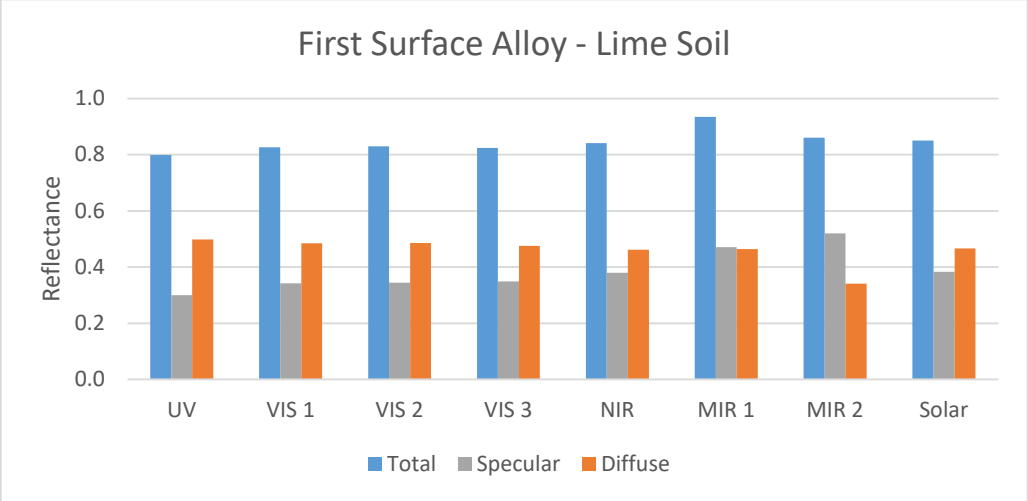

Figure 14 – Mean reflectance values of a first surface alloy mirror soiled using lime soil

3.2.3 Multispectral Soiling Plots

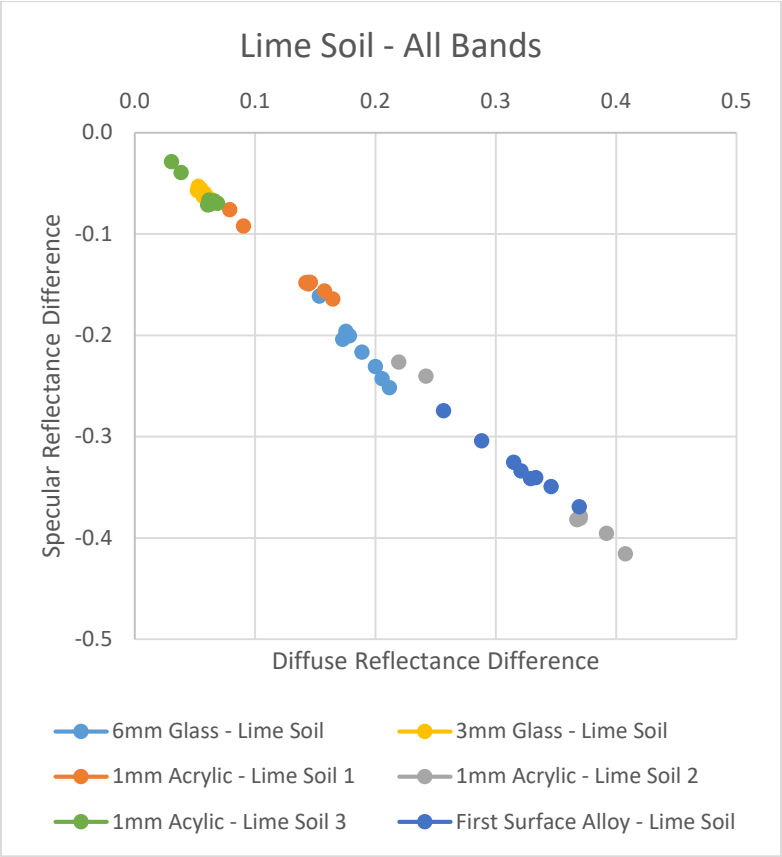

Figure 15 – Soiling reflectance differences for lime soil showing all reflectometer bands

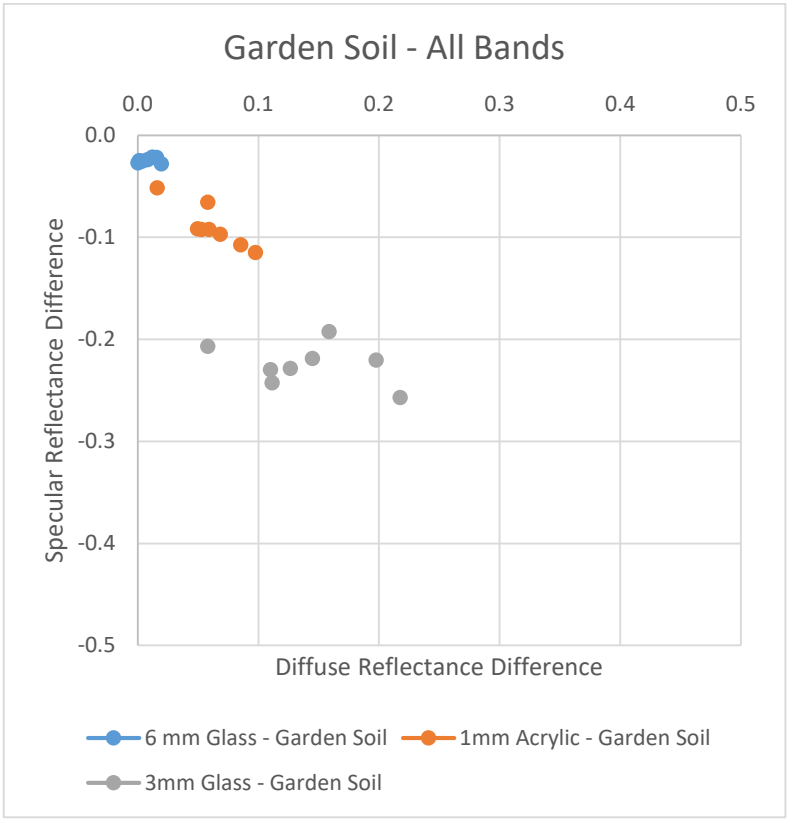

Figure 16 – Soiling reflectance differences for garden soil showing all reflectometer bands

3.2.4 Linear Regression of Soiling Plots

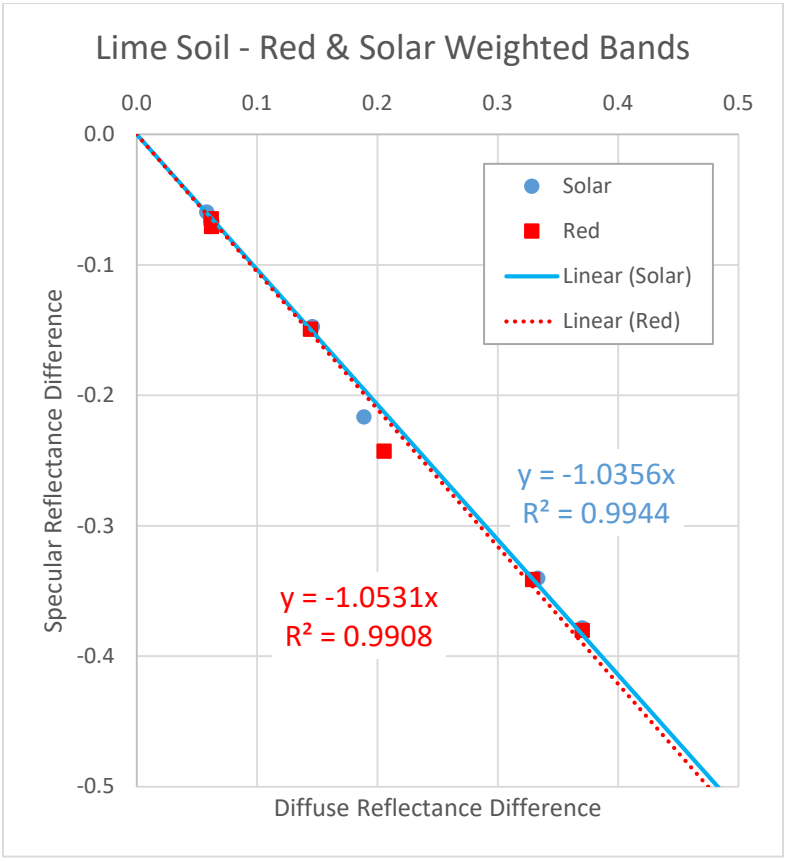

Figure 17 – Soiling linear regressions for red and solar weighted bands with lime soil

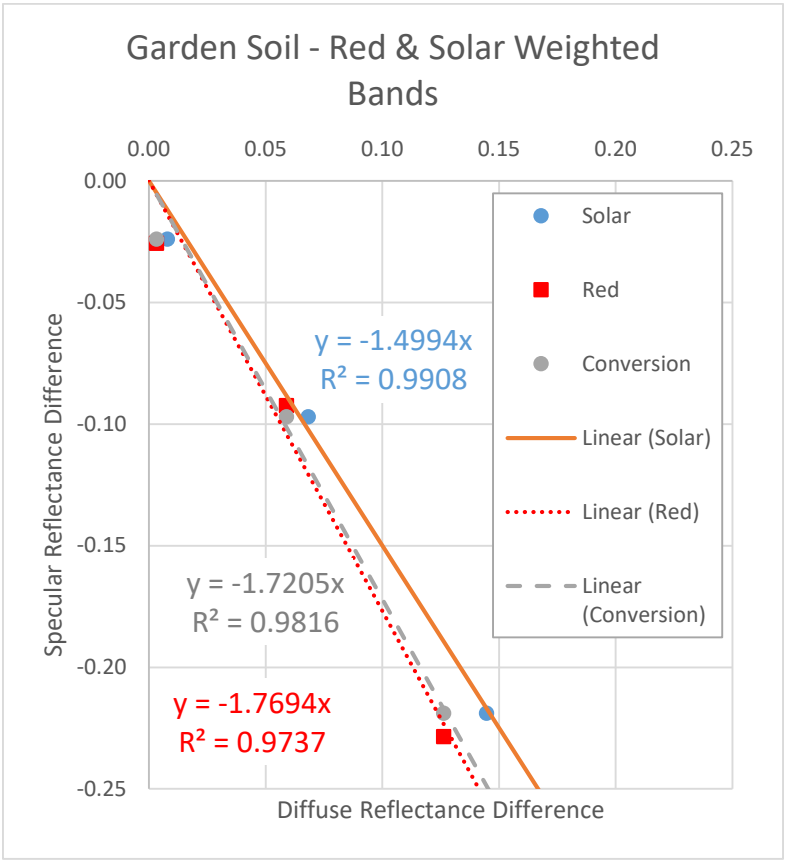

Figure 18 – Soiling linear regressions for red and solar weighted bands with garden soil

3.3 DISCUSSION

Looking at the spectral signatures of the mirror surface types (Figures 4-14), we can see clear benefits between them. Although this is by no means a comprehensive sample of surface types, it was found that surfaces with no or little material in front of the reflective surface tend to perform better considering the solar weighted specular reflectance. It was also noted that the drop in total reflectance due to soiling due from the lighter shade soil (lime soil), generally resulted in higher increase is diffuse reflectance than the darker colour soil (garden soil). This was an intuitive result, as you would expect the darker soil to absorb more energy due to the fact that it appears dark. This also held in the solar weighted bands.

Looking at the multispectral soiling plots (Figures 15 & 16), we can see that the relationship between change in diffuse reflectance and change in specular reflectance appears to be well correlated for the light-coloured lime soil across all mirror surface types. This suggests that it is unlikely that the lime soil and the mirror surface will experience refractive effects that will limit our ability to estimate specular reflectance by measuring the diffuse reflectance. Unfortunately, the same cannot be said for the darker garden soil.

Looking at the linear regressions plotted for the red bands (VIS 3) and solar weighed bands (Figures 17-18) we can see that again as the change in diffuse reflection from the clean state versus the drop in specular reflection from the clean state are well correlated for the lime soil. This is ideal for using optical band sensors to estimate a solar weighted band reflectance. The dark garden soil again shows are clear split between red and solar weighted bands. As long as this dust can be optically characterised as such, this is suitable for remote sensing. However, some sensitivity is lost due to abortion incident energy, as is evident by the steeper linear correlation plotted. More data is desired for the dark coloured soils in order to better define the conversion between red band diffuse reflectance and solar weighted band.

4 REMOTE SENSING IMAGE DATA

4.1 METHODS

The preliminary image data was acquired using a Nikon D3000 digital single-lens reflex (DSLR) camera. This camera equipped with a 10 megapixel, 12-bit RBG CCD image sensor. The flash is used to achieve active sensing of the diffuse reflections from the mirror (see Figure 19). The lens used was an 18-55mm focal length and f/3.5-5.6G aperture. The horizontal angle of view is approximately 65° horizontally and 45° vertically using an 18mm focal length. A tripod was set-up with the camera view normal to the mirror surface at a perpendicular distance of 1 m between the lens and top edge of the mirror. Importantly, these experiments were performed outside at night so as to avoid optical interference.

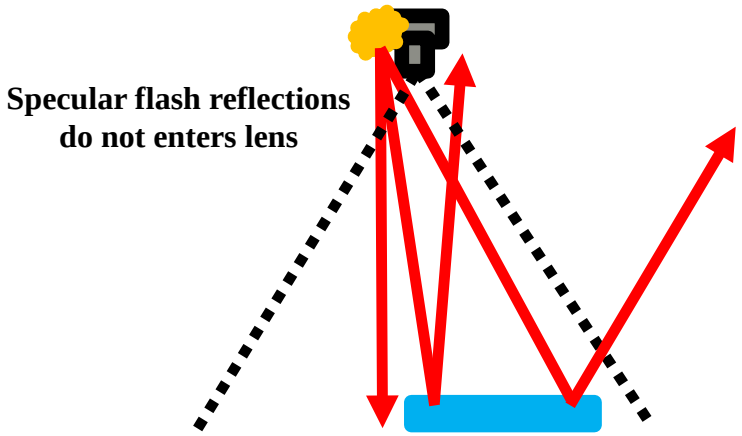

Figure 19 - Image data acquisition setup

4.2 RESULTS

4.2.1 Clean Mirror

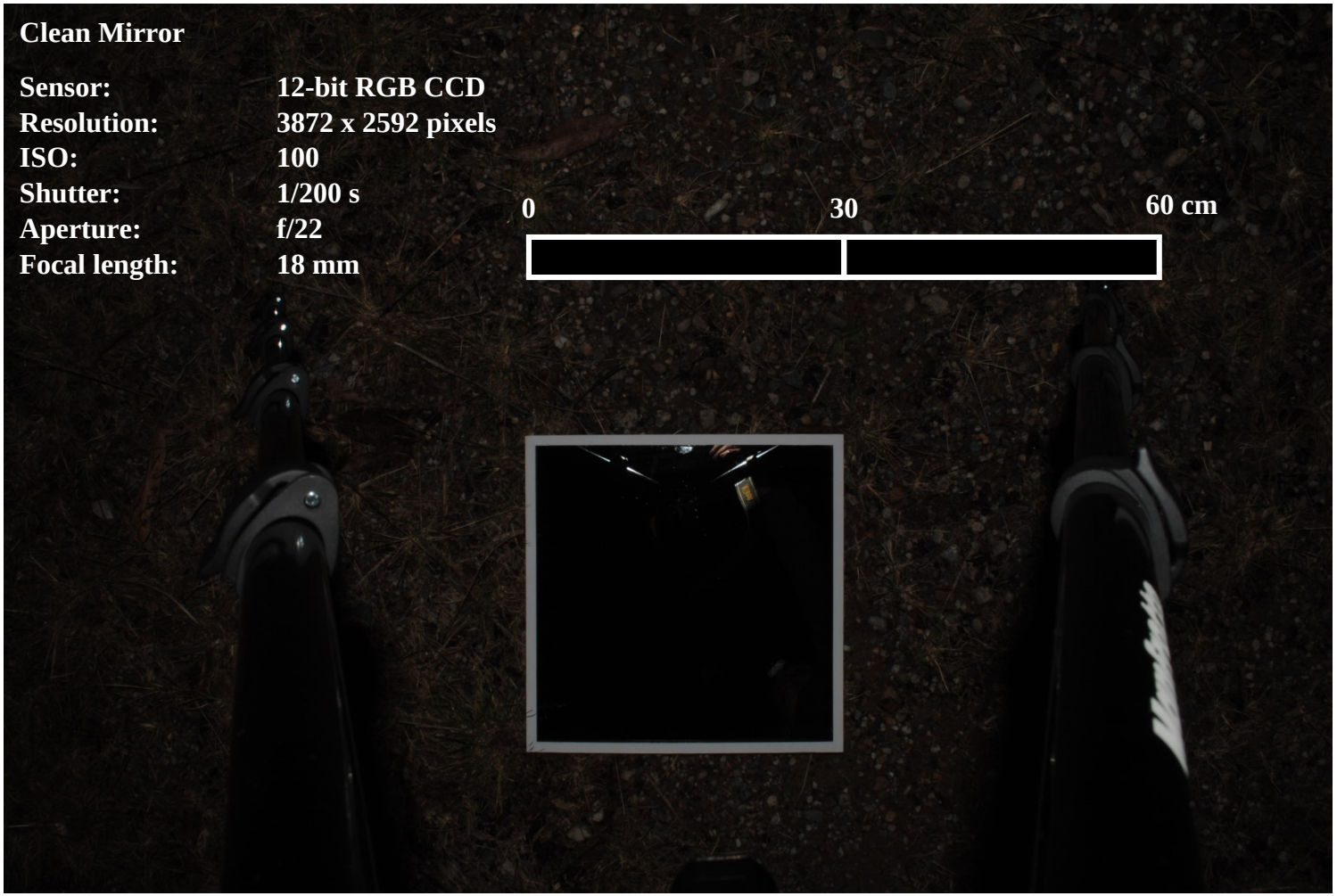

Figure 20 – Raw true-colour image of a clean 30 x 30 cm, 6mm glass mirror

4.2.2 Soiled Mirror – Lime Soil

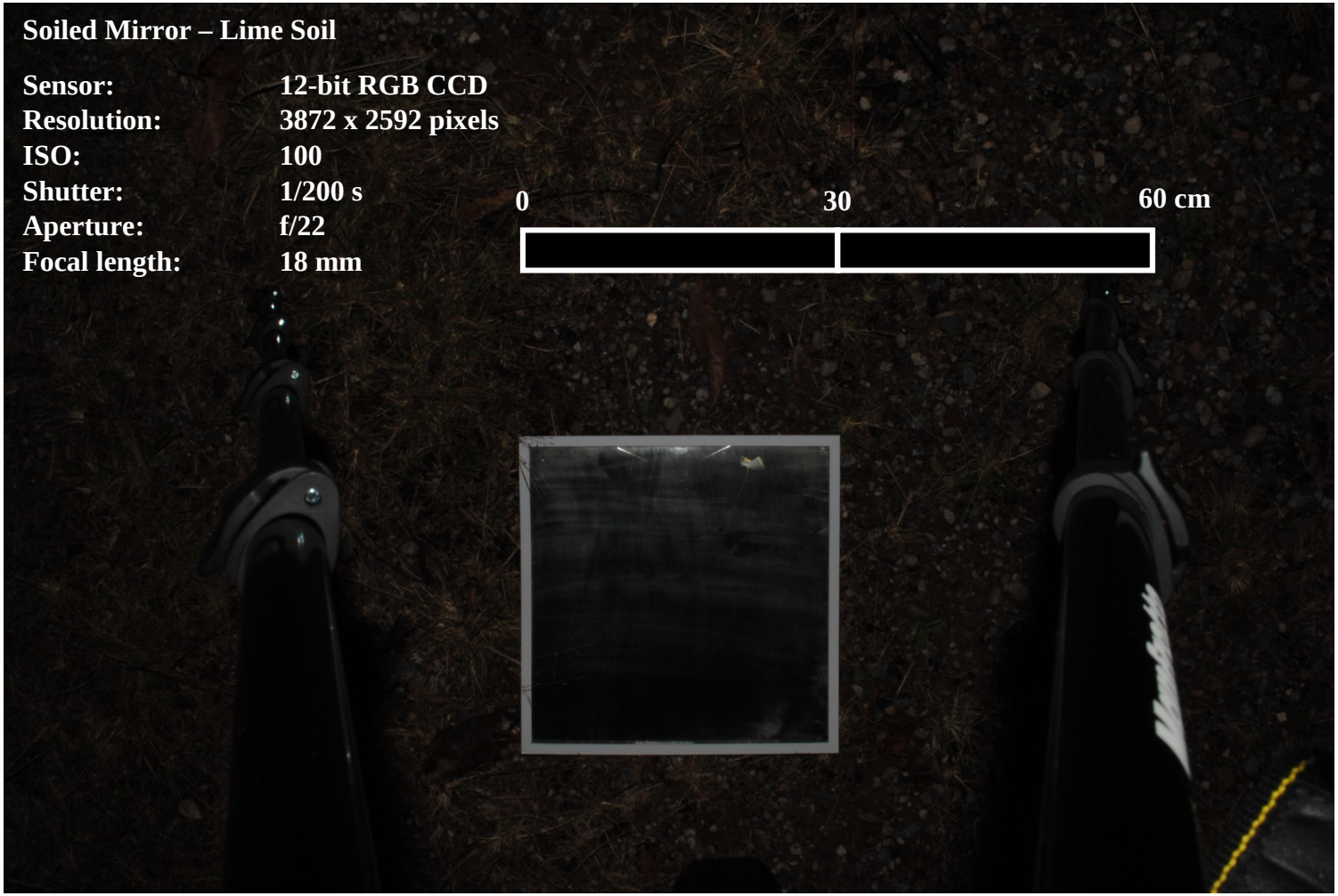

Figure 21 – Raw true-colour image of a soiled (lime soil) 30 x 30 cm, 6mm glass mirror

4.2.3 Soiled Mirror – Garden Soil

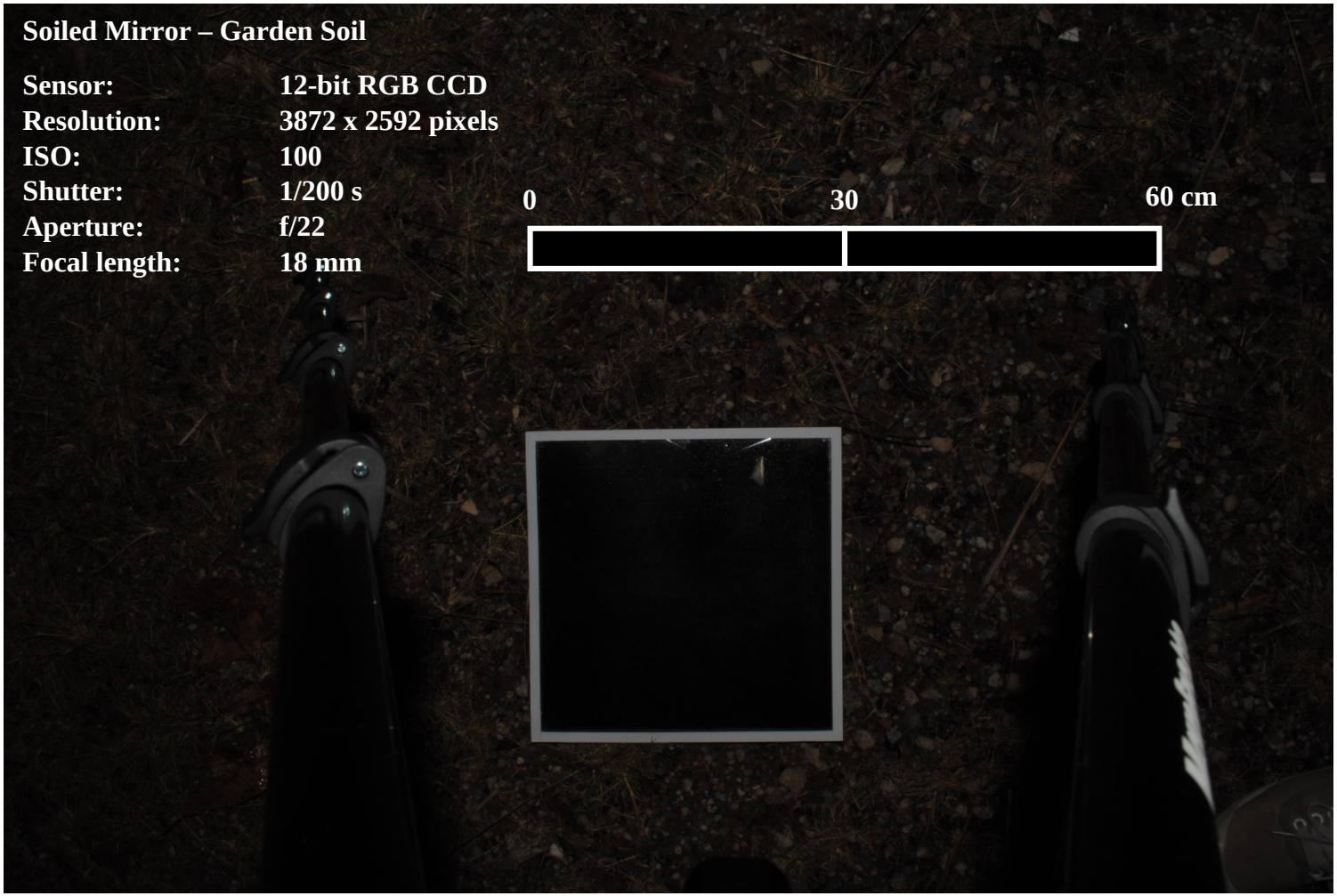

Figure 22 – Raw true-colour image of a soiled (garden soil) 30 x 30 cm, 6mm glass mirror

4.3 DISCUSSION

Some visible changes are visible in the simulated UAV-perspective image data (Figures 20-22), most notably the soiled mirror using lime soil (Figure 21). Some background interference is also visible, such as the tripod legs seen in the top of the mirror. It can also be seen that the top side of the mirror has a higher intensity reflection. This is most likely due to the different amounts of incident irradiance received, which is a function of the indecent angle of the flash as well as its power distribution. The next section aims to described this effect as well as estimate the diffuse and specular reflectance of the mirror surface.

5 IMAGE PROCESSING

5.1 METHODS

In order to convert the raw digital numbers obtained from the image data into physical reflectance values we require either a calibration surface in the image, or high detailed radiometric model combined with geometry data. As a preliminary look, a diffuse cardboard border of 1 cm in width was fixed to the mirror surfaces. The cardboard was characterised using the 410-Solar reflectometer. As can be seen by the spectral signature of the cardboard in Figure 23, the red average (VIS 3) and solar weighted bands have a diffuse reflectance of approximately 83%, with very little specular reflectance. This therefore provides a sensitive calibration target for converting the digital numbers to diffuse reflectance. This primary software used to perform the image processing was ENVI. Python was also used with the open source image processing library, *scikit-image*, to evaluate horizontal and vertical intensity profiles.

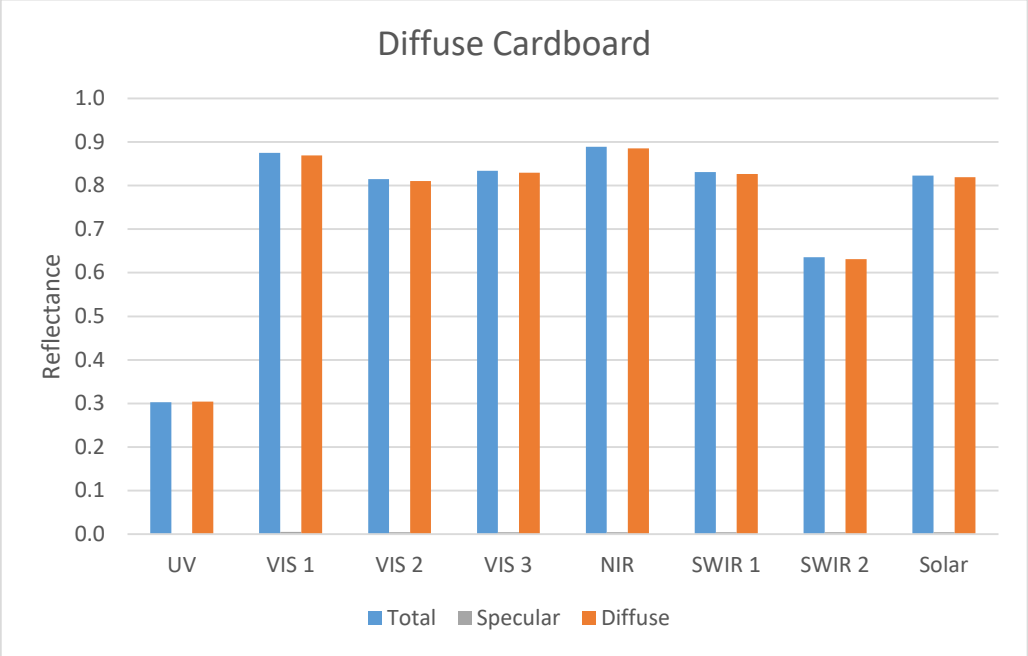

Figure 23 – Nikon D3000 relative flash power distribution as measured using a diffuse sheet

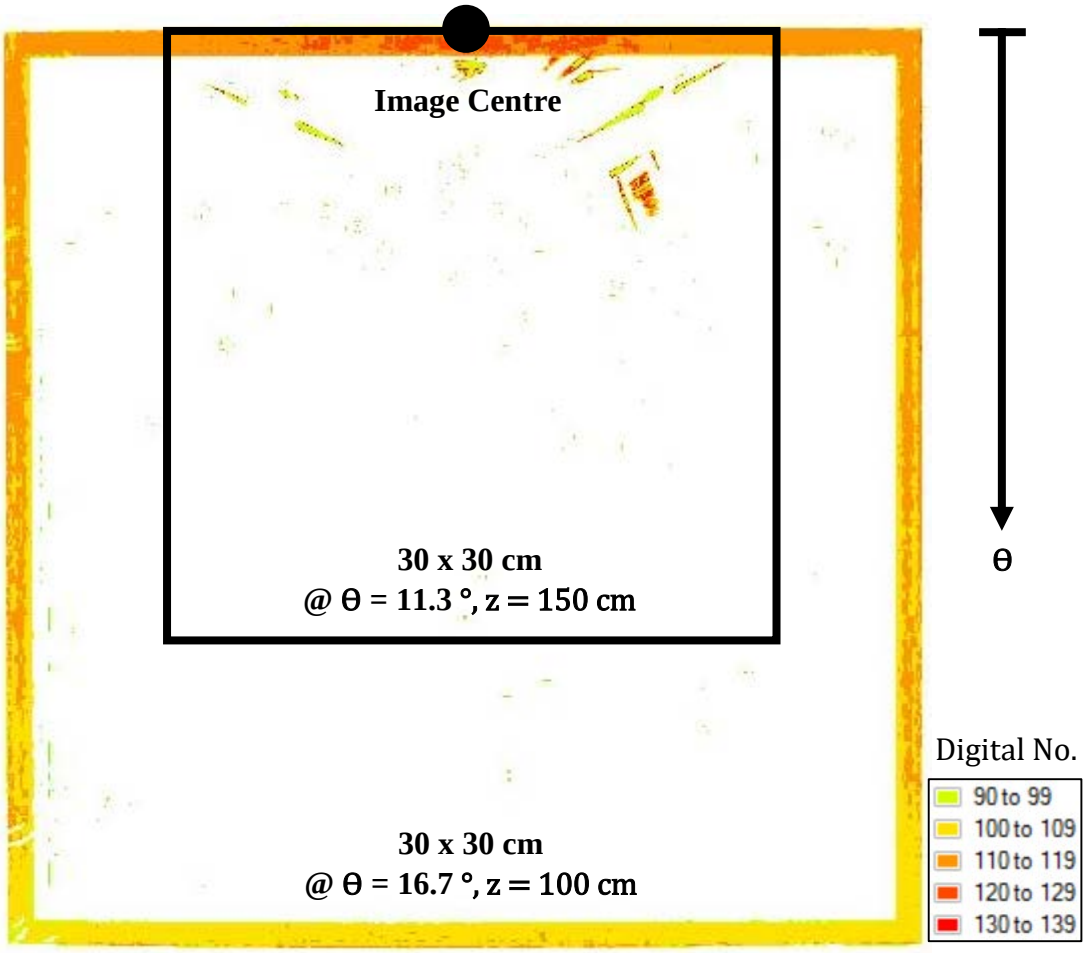

Figure 24 – Nikon D3000 flash power distribution as measured using a diffuse cardboard border

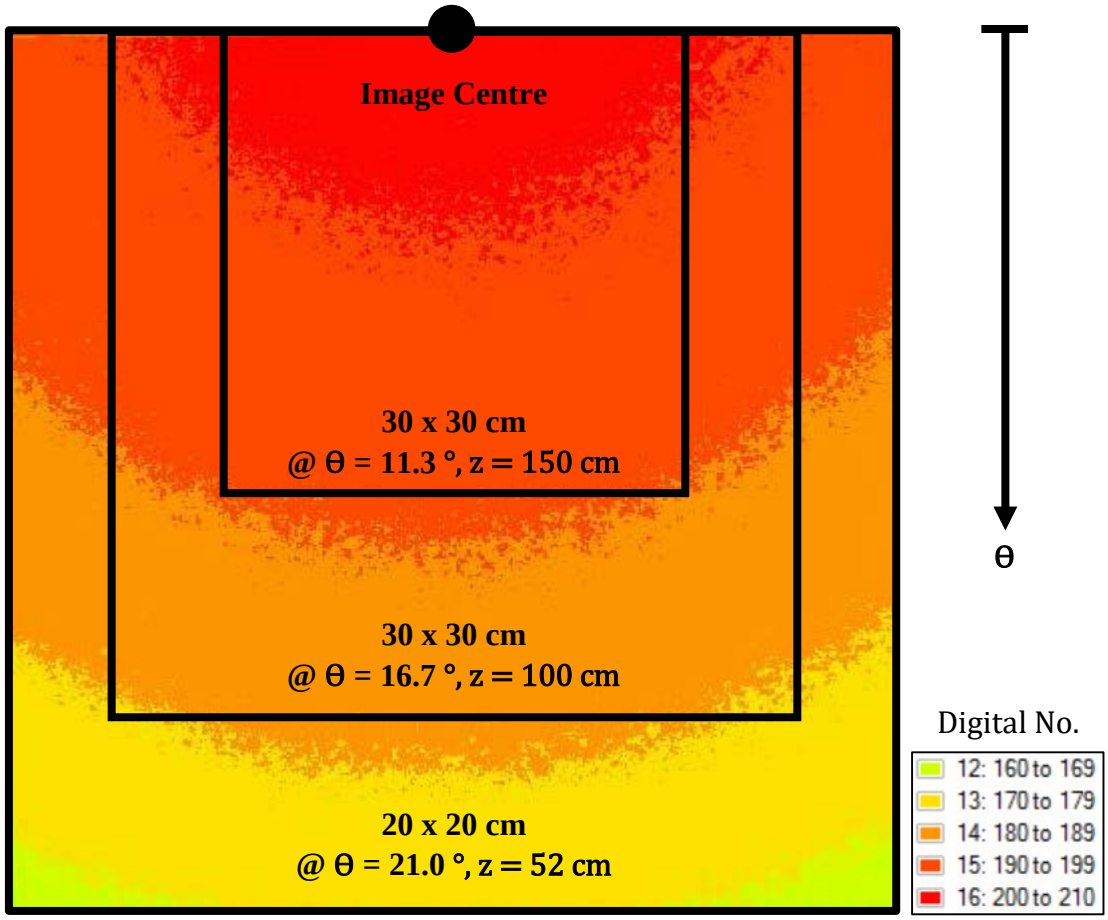

Figure 25 – Nikon D3000 flash power distribution as measured using a diffuse cardboard sheet

5.2 RESULTS

5.2.1 Clean Mirror

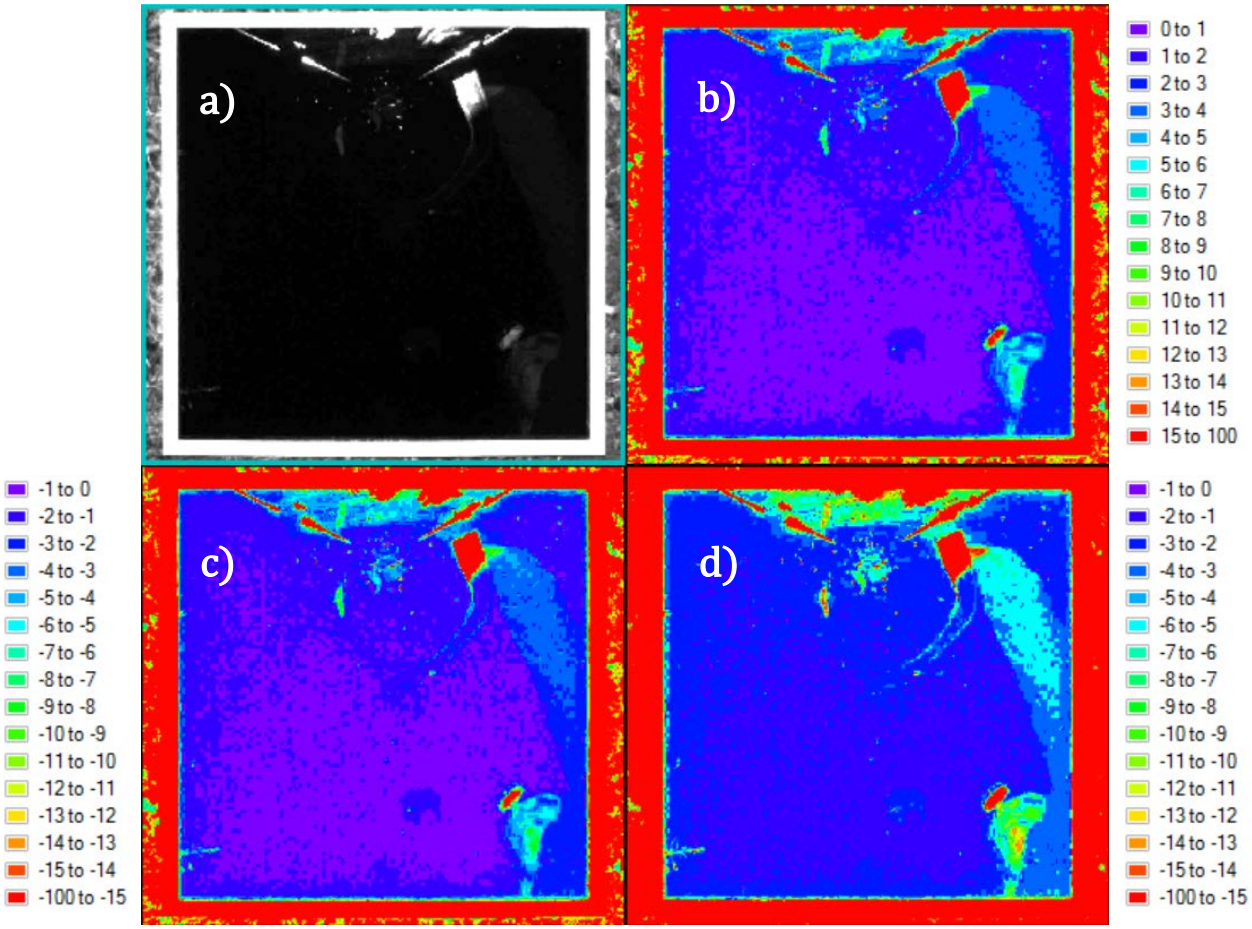

Figure 26 – Clean mirror red-band data: a) raw greyscale; b) diffuse reflectance classification; c) specular reflectance classification using lime soil regression; d) specular reflectance classification using garden soil regression

5.2.2 Soiled Mirror – Lime Soil

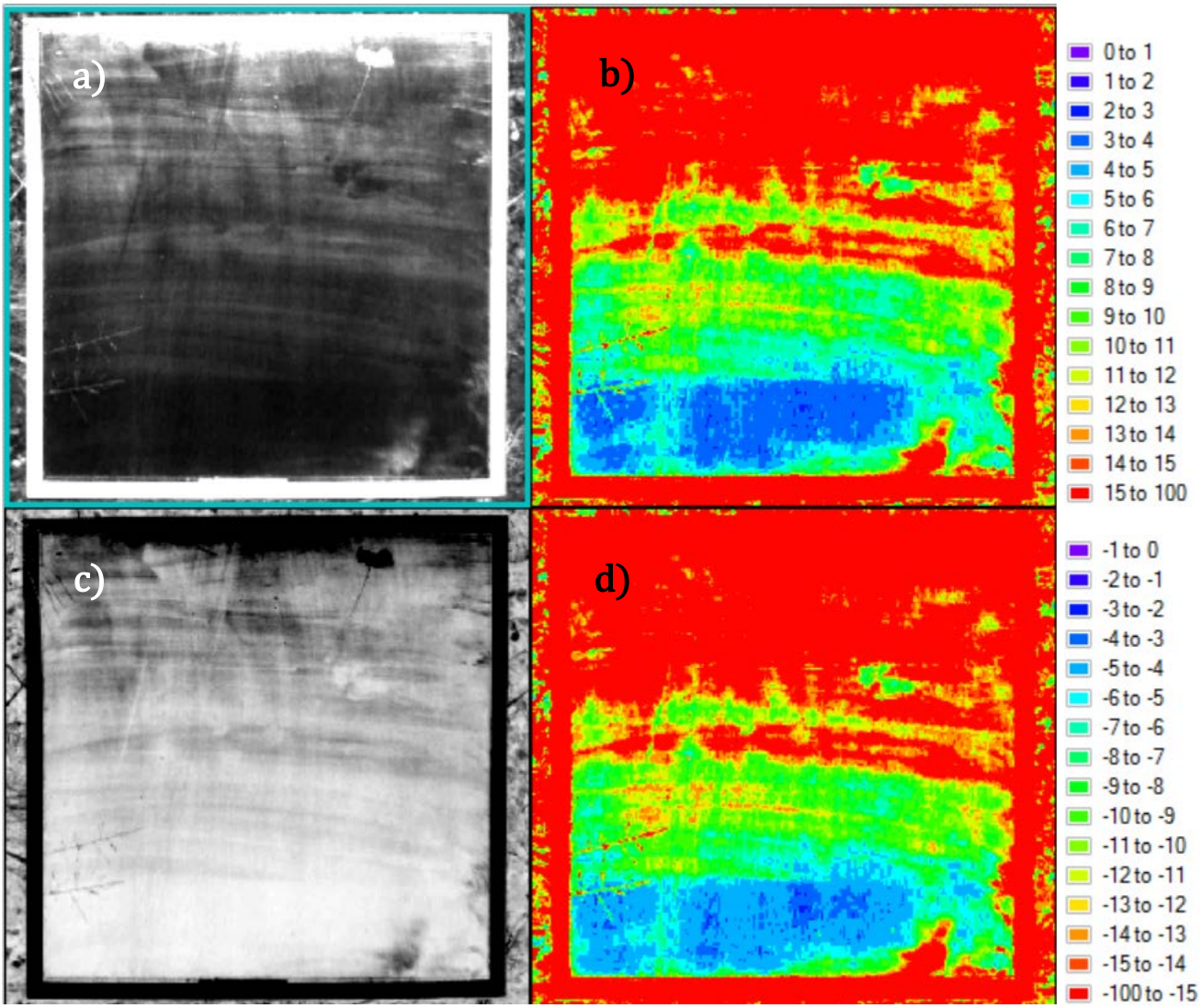

Figure 27 – Lime-soiled mirror red-band data: a) diffuse greyscale; b) diffuse reflectance classification; c) specular reflectance greyscale; d) specular reflectance classification

5.2.3 Soiled Mirror – Garden Soil

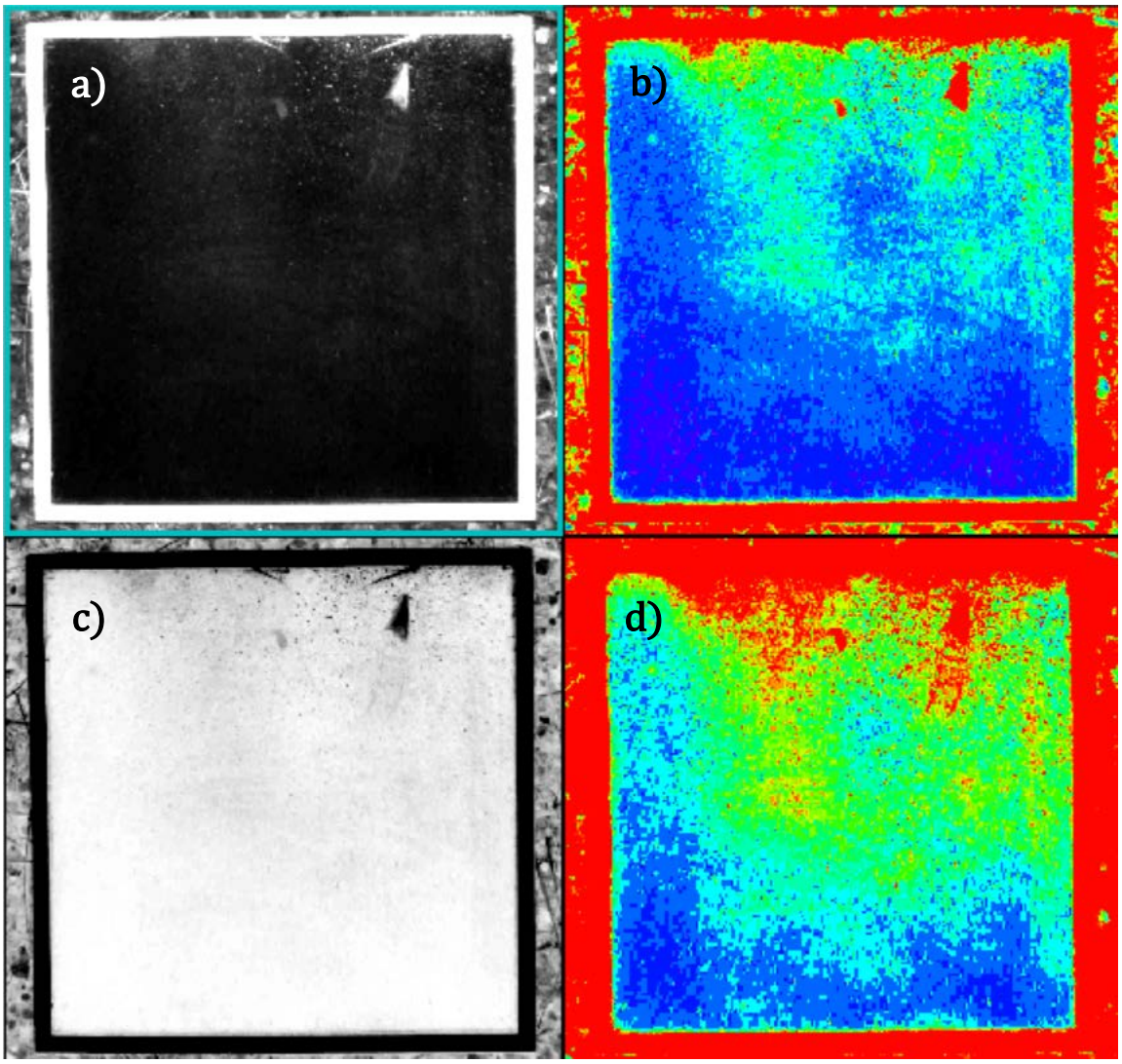

Figure 28 – Garden-soiled mirror red-band data: a) diffuse greyscale; b) diffuse reflectance classification; c) specular reflectance greyscale; d) specular reflectance classification

5.2.4 Statistics Summary

	Digital Number		**Diffuse Reflectance**		**Specular Reflectance**			
	Unprocessed 8-bit Range		Mean Border Calibration		Lime Regression		Garden Regression	
	Mean	Standard Deviation	Mean	Standard Deviation.	Mean	Standard Deviation	Mean	Standard Deviation
Clean	3.40	11.48	2.59	8.74	- 2.72	9.21	- 4.46	15.04
Soiled - Lime Soil	18.51	13.80	14.39	10.73	-15.16	11.3	n/a	n/a
Soiled - Garden Soil	6.48	5.77	5.00	4.41	n/a	n/a	- 8.60	7.59

Table 2 – Statistics computed for clean and soiled mirror surfaces

5.3 DISCUSSION

The plots seen in Figures 24 and 25 described the angular power distribution of the flash. The smaller squares are shown to gain a sense of how the power distribution will vary for objects at different distances from the lens plane. As the surface moves further from the lens, the distortion is reduced and the calibration can be improved. However, less energy is also received, meaning more flash power is required to achieve the same sensitivity.

In order to estimate the diffuse reflectance of the mirror surface, the border area was manually selected and an averaged. The pixel values were then systematically divided by the mean border value and multiplied by 82, the measured diffuse reflectance or the border. The pixel values, now in units of diffuse reflectance, were then multiplied by the corresponding linear regression coefficients calculated previously, to obtain units of change in specular reflectance. The plots in Figures 26-28 were not normalised for the clean mirror noise values. This is likely to reduce some of the error in the current plots (which were processed without checking for clean-mirror background values).

It is evident that the power distribution of the flash is significantly distorting the reflectance values as the gradient from top to bottom is not due to having more soil towards the top of the mirror. However, from the results plotted a good idea soiling can be obtained. The clean heliostat can be clearly distinguished from both the lime soiled heliostat and the garden siled heliostat. This was not as evident looking at the raw unprocessed images, especially so for the garden soiled mirror. The statistical results in Table 2 shows that the mean reductions in specular reflectance are less than 5% for the clean mirror. All soiled results show a reduction in specular reflectance of greater than 5%. Although this is useful as a qualitative threshold, the uncertainty in the clean mirrors are significant in relation to when you would to consider cleaning heliostats.

In addition to formulating an irradiance model of the flash and integrating it into the image processing, validation must be performed by taking reflectance measurements in parallel to acquiring the images. This was not achieved due to the limitations in availability of the reflectometer after business hours and the requirement for the images to be captured at night (so as to isolate optical interference). Alternatively, highly-diffuse lighting sources may be investigated. This would not negate the requirement for a calibration surface within the image, but it would likely reduce the distortions that result from most standard camera flashes. In an automated UAV system that simultaneously mapped the environment (such as a LiDAR system) distance and angle based models could be investigated.

6 CONCLUSION

A remote sensing technique has been developed that makes use of the relationship between the changes in specular and diffuse reflectance of soiled reflectors. This technique is shown to have best sensitivity in environments with light-coloured, diffuse dust compositions. For such environments, the increase in diffuse reflectance, as measured by an active visible-band optical imaging sensor, can be used to accurately estimated the reduction in solar-weighted specular reflectance. However, dark-coloured, absorbing soils require further data to optically characterise, before being able to apply the same remote sensing technique.

The image processing results improved the qualitative assessment of soiling from the raw images. The short-term future work required to develop this technique will involve validating these results as well as addressing the issue of non-diffuse lighting. Long-term work would be focused on automating the image processing tasks, as well as integrating the remote sensing technique into a UAV.

REFERENCES

AMERICAN SOCIETY FOR TESTING AND MATERIALS 2012. Standard Tables for Reference Solar Spectral Irradiances: Direct Normal and Hemispherical on 37° Tilted Surface. ASTM International.

AMERICAN SOCIETY FOR TESTING AND MATERIALS 2012. Standard Test Method for Solar Absorptance, Reflectance, and Transmittance of Materials Using Integrating Spheres. United States of America: American Society for Testing and Materials.

AUSTRALIAN SOLAR THERMAL RESEARCH INITIATIVE 2014. ASTRI Annual Report. Newcastle: ASTRI.

AUSTRALIAN SOLAR THERMAL RESEARCH INITIATIVE 2015. ASTRI Annual Report. Newcastle: ASTRI.

COVENTRY, J., PYE, J., ANDRAKA, C., BLANCO, M. & FISHER, J. 2014. Sodium receivers for solar power towers: a review. *In:* ASTRI (ed.) *Sodium receivers.*

DNP DENMARK 2016. Standard and Front Surface Mirrors.

FERNÁNDEZ-RECHE, J. 2006. Reflectance measurement in solar tower heliostats fields. *Solar Energy,* 80**,** 779-786.

KALOGIROU, S. A. 2004. Solar thermal collectors and applications. *Progress in Energy and Combustion Science,* 30**,** 231-295.

LOOK, D. C. 1965. Diffuse Reflection from a Plane Surface*. *Journal of the Optical Society of America,* 55**,** 1628-1632.

SPARKES, D. 2016. 'Tantalisingly close': is solar thermal energy ready to replace coal-fired power? *The Guardian*.

VAST SOLAR 2015. Project Overview & Update. Sydney: Vast Solar Pty Limited.

APPENDIX A – TABULATED REFLECTOMETER RESULTS

Test #	Test Description	UV 335-380 nm	VIS 1 400-540 nm	VIS 2 480-600 nm	VIS 3 590-720 nm	NIR 700-1100 nm	MIR 1 1000-1700 nm	MIR 2 1700-2500 nm	Solar Weighted
Mean Total Reflectance									
1	6mm Glass - Clean	0.590	0.798	0.863	0.819	0.647	0.670	0.731	0.733
7	6mm Glass - Lime Soil	0.582	0.767	0.823	0.782	0.627	0.649	0.700	0.705
13	6mm Glass - Garden Soil	0.571	0.773	0.836	0.796	0.638	0.665	0.722	0.717
Mean Diffuse Reflectance									
1	6mm Glass - Clean	0.089	0.127	0.136	0.130	0.102	0.108	0.109	0.116
7	6mm Glass - Lime Soil	0.243	0.327	0.348	0.336	0.278	0.287	0.282	0.305
13	6mm Glass - Garden Soil	0.088	0.128	0.136	0.134	0.114	0.124	0.129	0.124
Mean Specular Reflectance									
1	6mm Glass - Clean	0.500	0.670	0.727	0.688	0.545	0.562	0.621	0.617
7	6mm Glass - Lime Soil	0.339	0.440	0.475	0.446	0.349	0.362	0.418	0.401
13	6mm Glass - Garden Soil	0.483	0.645	0.700	0.663	0.524	0.541	0.593	0.593

Test #	Test Description	UV	VIS 1	VIS 2	VIS 3	NIR	MIR 1	MIR 2	Solar Weighted
		335-380 nm	400-540 nm	480-600 nm	590-720 nm	700-1100 nm	1000-1700 nm	1700-2500 nm	
Mean Total Reflectance									
29	3mm Glass - Clean	0.708	0.769	0.811	0.755	0.620	0.691	0.777	0.714
38	3mm Glass - Lime Soil	0.703	0.766	0.808	0.753	0.620	0.691	0.772	0.712
44	3mm Glass - Clean	0.703	0.767	0.809	0.753	0.620	0.691	0.777	0.713
48	3mm Glass - Garden Soil	0.553	0.647	0.678	0.651	0.586	0.668	0.737	0.638
Mean Diffuse Reflectance									
29	3mm Glass - Clean	0.009	0.012	0.012	0.011	0.008	0.011	0.012	0.010
38	3mm Glass - Lime Soil	0.066	0.075	0.078	0.073	0.061	0.066	0.064	0.069
44	3mm Glass - Clean	0.009	0.013	0.013	0.012	0.009	0.011	0.013	0.011
48	3mm Glass - Garden Soil	0.066	0.123	0.124	0.138	0.168	0.209	0.230	0.156
Mean Specular Reflectance									
29	3mm Glass - Clean	0.699	0.757	0.799	0.744	0.612	0.681	0.765	0.703
38	3mm Glass - Lime Soil	0.636	0.691	0.730	0.680	0.559	0.625	0.708	0.644
44	3mm Glass - Clean	0.694	0.754	0.796	0.742	0.611	0.680	0.765	0.702
48	3mm Glass - Garden Soil	0.487	0.524	0.553	0.513	0.418	0.460	0.507	0.483

Test #	Test Description	UV 335-380 nm	VIS 1 400-540 nm	VIS 2 480-600 nm	VIS 3 590-720 nm	NIR 700-1100 nm	MIR 1 1000-1700 nm	MIR 2 1700-2500 nm	Solar Weighted
Mean Total Reflectance									
4	1mm Acrylic - Clean	0.515	0.863	0.863	0.849	0.858	0.872	0.494	0.830
11	1mm Acrylic - Lime Soil	0.518	0.859	0.857	0.845	0.860	0.873	0.492	0.829
16	1mm Acrylic - Garden Soil	0.479	0.823	0.821	0.816	0.837	0.854	0.486	0.801
26	1mm Acrylic - Clean	0.534	0.870	0.870	0.853	0.860	0.874	0.497	0.834
35	1mm Acrylic - Lime Soil	0.527	0.856	0.857	0.843	0.856	0.866	0.499	0.826
54	1mm Acrylic - Lime Soil	0.563	0.901	0.901	0.877	0.874	0.878	0.495	0.853
57	1mm Acrylic - Clean	0.561	0.909	0.911	0.886	0.875	0.879	0.496	0.857
Mean Diffuse Reflectance									
4	1mm Acrylic - Clean	0.009	0.008	0.007	0.006	0.004	0.003	0.004	0.006
11	1mm Acrylic - Lime Soil	0.088	0.152	0.150	0.151	0.162	0.168	0.094	0.152
16	1mm Acrylic - Garden Soil	0.025	0.060	0.057	0.065	0.090	0.101	0.062	0.074
26	1mm Acrylic - Clean	0.012	0.009	0.008	0.007	0.005	0.004	0.003	0.006
35	1mm Acrylic - Lime Soil	0.231	0.377	0.376	0.377	0.397	0.411	0.245	0.377
54	1mm Acrylic - Lime Soil	0.053	0.077	0.076	0.074	0.074	0.075	0.044	0.073
57	1mm Acrylic - Clean	0.023	0.016	0.015	0.012	0.008	0.006	0.005	0.011
Mean Specular Reflectance									
4	1mm Acrylic - Clean	0.506	0.855	0.855	0.843	0.854	0.869	0.490	0.824
11	1mm Acrylic - Lime Soil	0.430	0.708	0.708	0.694	0.698	0.705	0.398	0.677
16	1mm Acrylic - Garden Soil	0.454	0.763	0.764	0.751	0.747	0.754	0.424	0.727
26	1mm Acrylic - Clean	0.523	0.861	0.862	0.847	0.855	0.871	0.493	0.828
35	1mm Acrylic - Lime Soil	0.296	0.479	0.480	0.466	0.460	0.455	0.253	0.450
54	1mm Acrylic - Lime Soil	0.510	0.824	0.824	0.803	0.800	0.803	0.451	0.780
57	1mm Acrylic - Clean	0.538	0.893	0.895	0.874	0.867	0.873	0.490	0.846

Test #	Test Description	UV 335-380 nm	VIS 1 400-540 nm	VIS 2 480-600 nm	VIS 3 590-720 nm	NIR 700-1100 nm	MIR 1 1000-1700 nm	MIR 2 1700-2500 nm	Solar Weighted
Mean Total Reflectance									
32	First Surface Alloy - Clean	0.816	0.837	0.842	0.836	0.845	0.934	0.876	0.857
41	First Surface Alloy - Lime Soil	0.799	0.826	0.830	0.824	0.841	0.935	0.861	0.850
Mean Diffuse Reflectance									
32	First Surface Alloy - Clean	0.242	0.169	0.164	0.146	0.116	0.095	0.052	0.133
41	First Surface Alloy - Lime Soil	0.499	0.484	0.485	0.475	0.462	0.464	0.341	0.467
Mean Specular Reflectance									
32	First Surface Alloy - Clean	0.574	0.668	0.678	0.690	0.729	0.839	0.824	0.724
41	First Surface Alloy - Lime Soil	0.300	0.342	0.344	0.349	0.379	0.470	0.520	0.383

APPENDIX B – IMAGE DATA PROFILING CODE (PYTHON 3)

```
# profile_vertical.py
'''
Plot Vertical Grayscale Intensity Profile
from JPG Image
'''

# Functions
from scipy.misc import imread
from skimage.io import imshow, show
from skimage.color import rgb2gray
from skimage.measure import profile_line
from pylab import title, xlabel, ylabel, grid, plot, xlim,
contour, legend, show
from numpy import zeros

# Load Image
file = 'data.jpg'
img = imread(file)

# Convert Image to Grayscale (2D array)
img_gray = rgb2gray(img)

# Show Grayscale Image
imshow(img_gray)
show()

# Generate Intensity Profile
x = int(input('x = '))
y0 = int(input('y0 = '))
y1 = int(input('y1 = '))
dx = 1
img_profile = profile_line(img_gray, (y0, x), (y1, x), dx)

# Plot Intensity Profile
pixel = zeros((y1-y0)+1, int)
for i in range(0, len(pixel)):
    pixel[i] = y0 + i
xlabel('Pixel (Top to Bottom)')
ylabel('Grayscale Pixel Intensity')
plot(pixel, img_profile, label=file)
legend(loc='best')
show()
```